日本磁気学会
ISSN 2432-0250
Journal of the Magnetics Society of Japan
Electronic Journal URL: https://www.jstage.jst.go.jp/browse/msjmag

Vol.42 No.4 2018

Journal

JOURNAL OF THE MAGNETICS SOCIETY OF JAPAN

Vol.42 No.4 2018

日本磁気学会

ISSN 2432-0250

HP: http://www.magnetics.jp/ e-mail: msj@bj.wakwak.com
Electronic Journal: http://www.jstage.jst.go.jp/browse/msjmag

JMSJ

COMSOL MULTIPHYSICS®

有限要素法解析ソフトウェア COMSOL Multiphysics®

マルチフィジックスの進化論

無制限・強連成で実現象に即したシミュレーション事例のご紹介

COMSOLご紹介セミナー

COMSOL Multiphysics®で、電磁界に加えて、構造・機械・振動・流体・伝熱、さらに加えて化学反応工学まで連成できるシミュレーションを始めませんか？

東京(神田) 会場:7月11日、10月24日、19年1月23日 13:30開始～16:30終了 (当日、個別のご相談も承ります)

※埼玉県さいたま市と福島での開催を計画中です

参加費用：**無料** (事前申し込み制)

詳細とお申し込みはコチラ：
http://www.kesco.co.jp/comsol_intro.html

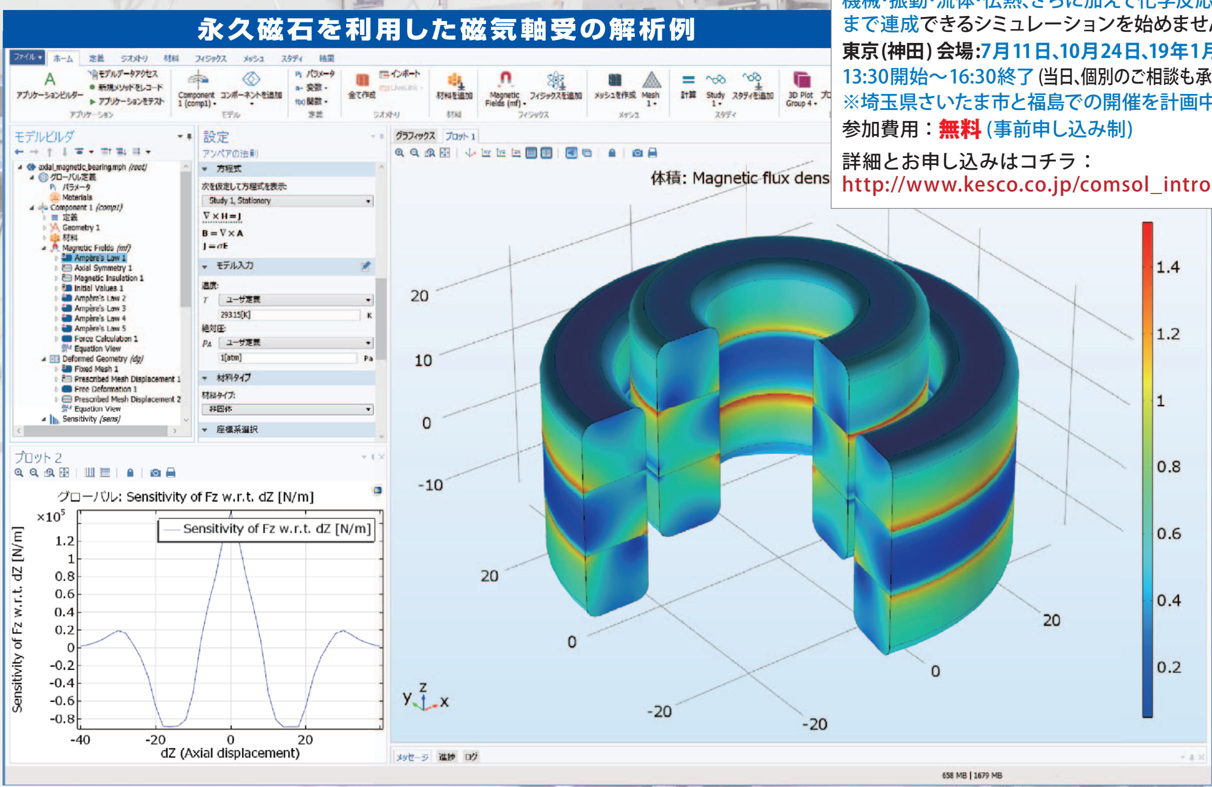

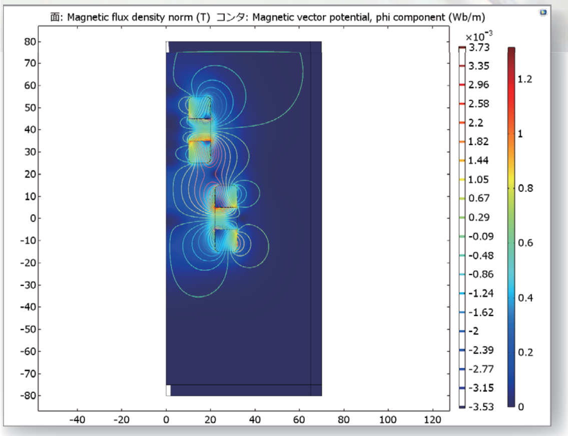

永久磁石を使用した磁気軸受

永久磁石を使用した軸受はターボ機械、ポンプ、モータ、発電機やフライホイール式エネルギー貯蔵システムなど、様々な分野で使用されています。非接触かつ潤滑不要で保守整備を大幅に省略できる点は、従来の機械式ベアリングと比べて重要なメリットです。この例では、軸方向の永久磁石軸受の磁気力と剛性などの設計パラメータを計算する方法を示しています。

※AC/DCモジュールはCOMSOL Multiphysicsと併用するアドオン製品です。

AC/DC モジュールの適用例

- AC/DC 電流分布、電場分布
- バイオヒーティング
- コイルとソレノイド
- SPICE 回路とフィールドシミュレーション
- 接触抵抗
- 電磁両立性 (EMC) および電磁妨害 (EMI)
- 電磁力およびトルク
- 電磁力シールド
- 電気機械の変形
- ホール効果を利用したセンサ
- インシュレータ、コンデンサ、誘電体
- モータ、ジェネレータ、および他の電気機械
- 非線形材料
- 寄生容量とインダクタンス
- 永久磁石と電磁石
- 多孔質材料
- 抵抗および誘導加熱
- センサ
- 超伝導体
- 変圧器とインダクタ

COMSOL Multiphysics® なら、今まで不可能だった 3 種以上のマルチフィジックス解析を強連成で実現できます。30 日間全機能無料トライアル、無料の導入セミナー、1000種を超える世界の様々な事例をご提供いたします。詳しくは、下記の弊社営業部までお問い合せください。

COMSOL

http://www.comsol.jp

KESCO KEISOKU ENGINEERING SYSTEM
計測エンジニアリングシステム株式会社
http://www.kesco.co.jp/comsol/
Tel : 03-5282-7040 ・ Fax : 03-5282-0808

世界初！
高温超電導型VSM

新製品

世界初*、高温超電導マグネットをVSMに採用することで
測定速度 当社従来機1/20を実現。
0.5mm cube磁石のBr, HcJ高精度測定が可能となりました。

*2014年7月 東英工業調べ

測定結果例

高温超電導VSMによるNdFeB(sint.) 0.5mm cube BHカーブ

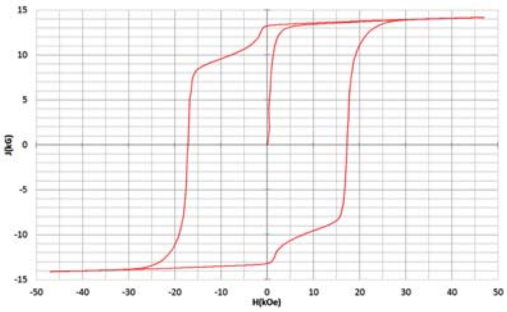

磁化測定レンジ：0.2emu
Br = 13.2kG　　HcJ = 17.2kOe

高温超電導VSMによるNdFeB(sint.) 1mm cube BHカーブ

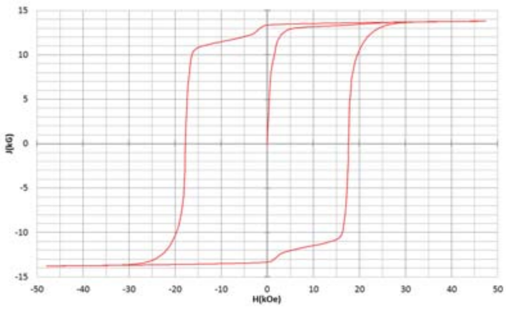

磁化測定レンジ：2emu
Br = 13.3kG　　HcJ = 17.7kOe

高温超電導VSMによるNdFeB(sint.) 4mm cube BHカーブ

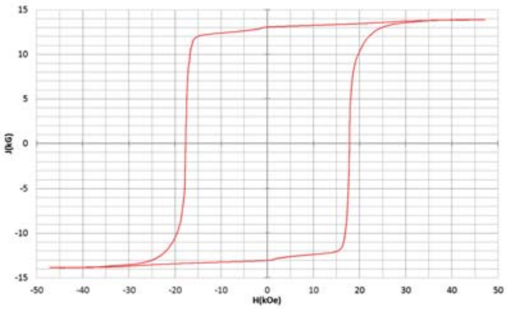

磁化測定レンジ：100emu
Br = 13.1kG　　HcJ = 17.8kOe

高速測定を実現

高温超電導マグネット採用により、高速測定を実現しました。Hmax= 5Tesla, Full Loop 測定が2分で可能です。
（当社従来機：Full Loop測定 40分）

小試料のBr,HcJ高精度測定

0.5mm cube磁石のBr,HcJ高精度測定ができ、表面改質領域を切り出しBr,HcJの強度分布等、微小変化量の比較測定が可能です。
また、試料の加工劣化の比較測定が可能です。

試料温度可変測定

−50℃～+200℃温度可変UNIT（オプション）

磁界発生部の小型化

マグネットシステム部寸法：0.8m×0.3m×0.3m

TOEI 東英工業株式会社
http://www.toeikogyo.co.jp
〒194-0035 東京都町田市忠生1-8-13
TEL：042-791-1211 FAX：042-792-0490
E-mail：sales@toeikogyo.co.jp

Journal of the Magnetics Society of Japan

Vol. 42, No. 4

Electronic Journal URL: https://www.jstage.jst.go.jp/browse/msjmag

CONTENTS

J. Magn. Soc. Jpn., **42**, 96-101 (2018)

<Paper>

Fabrication of $D0_{22}$-Mn_3Ge Thin Films by Alternate Sputtering Method

K. Watanabe*, H. Makuta**, M. Doi**, and T. Shima**

*Department of Applied Physics, Graduate School of Engineering, Tohoku Univ., *6-6-05 Aoba, Aoba-ku, Sendai 980-8579, Japan*

** Faculty of Engineering, Graduate School of Tohoku Gakuin Univ., *1-13-1, chuo, Tagajo, Miyagi 985-8567, Japan*

The crystal structure and magnetic properties of $D0_{22}$-Mn_3Ge thin films with a high perpendicular magnetic anisotropy constant (K_u) and a low magnetization (M_s) were investigated. $D0_{22}$-Mn_3Ge thin films were grown on the single crystal of MgO (100) substrates with Cr buffer layer using alternate sputtering method. The Mn_xGe thin films were prepared as $[Mn_x/Ge]_n$ multilayers ($2.8 \leq x \leq 3.7$) ($1 \leq n \leq 30$). We tried to fabricate $D0_{22}$-Mn_3Ge that shows a high K_u value of over 1.0×10^7 erg/cm^3 and a low M_s value of approximately 100 emu/cm^3 by the modulation of composition between Mn layer and Ge layer. As a result, $D0_{22}$-Mn_3Ge thin film with a high perpendicular magnetic anisotropy constant (K_u ~ ca. 1.0×10^7 erg/cm^3), a low saturation magnetization (M_s = 119 emu/cm^3) and good squareness from $[Mn_{3.5}/Ge]_{15}$ (T_s = 450°C, T_a = 500°C) multilayered film was obtained. Almost same magnetic properties were observed for the films of at n = 20, 25 without post annealing compared with the film annealed at T_a = 500°C. It is confirmed that increase of the repetition number n by the alternate sputtering method has a same effect of post annealing at 500°C.

Keywords: $D0_{22}$-Mn_3Ge, perpendicular magnetic anisotropy, coercivity, saturation magnetization, alternate sputtering method

1. Introduction

The magnetic thin films with a high perpendicular magnetic anisotropy (PMA) have been intensively studied in late years. These materials have been expected for the application of next generation hard disc drive (HDD) or spin transfer torque magnetic random access memory (STT-MRAM)[1]. Particularly, for the application of the STT-MRAM has much attention from the viewpoint of reduction of energy consumption in electronic devices. STT-MRAM is a non-volatile memory device including magnetic tunnel junctions (MTJs). The MTJ for STT-MRAM has been required that a high thermal stability (Δ), a tunnel magnetoresistance (TMR) ratio, and a low critical switching current (I_c) from the perspective of the ultra-large memory capacity with low power consumption. In order to realize a giga-bit class STT-MRAM, the diameter of memory cells must be less than 20 nm, the uniaxial magnetic anisotropy constant (K_u) must be larger than 5.0×10^6 erg/cm^3 which fulfill the relation of $\Delta = K_u V / k_B T > 60$[2)-4)]. A high-spin polarization is also very important issue to achieve a high TMR ratio, nearly full spin-polarized magnetic layers of the MTJs have been required[5)]. Furthermore, in order to realize the STT-MRAM with lower switching current, it has been required that magnetic materials having a small Gilbert damping constant (α) and a low saturation magnetization (M_s)[2)-4)]. However, conventional magnetic materials have not fulfilled these properties, such as perpendicularly magnetized CoFeB thin films[3),6)], $[Co/Pt]_n$ and $[Co/Pd]_n$ multilayers[7)-8)], CoCrPt thin films[9)], $[Co/Ni]_n$ multilayers[10)] and FePt thin films[11)].

In recent years, Mn-based intermetallic compounds have been attracted much attention such as $D0_{22}$-Mn_3Ga, $D0_{22}$-Mn_2Ga, $L1_0$-MnGa, $L1_0$-MnAl which show the tetragonal crystal structures[5),12)-25)], because they demonstrate a high K_u, a lower M_s, a small α. The Mn-Ga binary alloys have tetragonal crystal structures of $L1_0$ and $D0_{22}$, through 1:1-3:1 content ratio of manganese and gallium. The $L1_0$-MnGa[13)] shows ferromagnetism of M_s ~ 600 emu/cm^3 [14)]. On the other hand, $D0_{22}$-Mn_3Ga and $D0_{22}$-Mn_2Ga are ferrimagnetism with a low M_s ~ 250-360 emu/cm^3 [13)-15)]. Both of $L1_0$ and $D0_{22}$ crystal structures in Mn-Ga binary alloys show a high K_u ~ 1.2-2.35 $\times$ 10^7 erg/cm^3 [14)-15)] and a small α ~ 0.008-0.015[15)] and a relatively high spin polarization (P ~ 58%)[16)]. The $L1_0$-MnAl has a high K_u = 1.5 $\times$ 10^7 erg/cm^3 [17)-18)], a low M_s = 550 emu/cm^3 [19)-20)], a small α = 0.006[19)-20)]. These Mn-based intermetallic compounds have been well known as material of high potential for the STT-MRAM.

In remarkable Mn-based alloys, Mn-Ge binary alloys have been particularly attracted attention compared with other Mn-based compounds alloys. The Mn-Ge binary alloys have tetragonal crystal structure of $D0_{22}$, in the case of content ratio of manganese and germanium is approximately 3:1 ($D0_{22}$-Mn_3Ge). According to the recent many studies, $D0_{22}$-Mn_3Ge has been predicted that it possess a high K_u ~ 2.3 $\times$ 10^7 erg/cm^3 [5)], a low M_s ~ 180 emu/cm^3 [5)], a very small α ~ 0.0009 [5)], a very high P ~ 100% (Δ_1 bands)[21)]. In other experimental reports, the $D0_{22}$-Mn_3Ge film prepared on Cr buffered MgO (100) single crystal substrate has a high K_u ~ 1.2 $\times$ 10^7 erg/cm^3 [22)-24)], a low M_s ~ 120 emu/cm^3 [22)-24)] has been reported. Therefore, it is thought that $D0_{22}$-Mn_3Ge is a very promising magnetic material for STT-MRAM[25)].

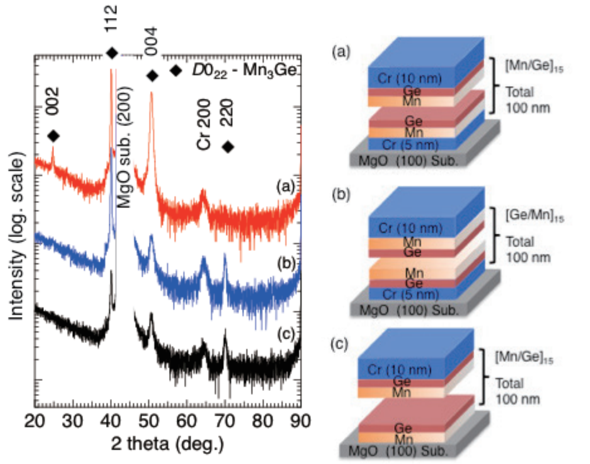

Fig. 1 XRD patterns and film structures for $[Mn/Ge]_{15}$ multilayered films.
(a) MgO sub. / Cr / $[Mn/Ge]_{15}$ (T_s = 450ºC) / Cr
(b) MgO sub. / Cr / $[Ge/Mn]_{15}$ (T_s = 450ºC) / Cr
(c) MgO sub. / $[Mn/Ge]_{15}$ (T_s = 450ºC) / Cr

In this study, we focused on the preparation technique of alternate sputtering method, which enables superior the control of interface and the content compared with co-sputtering method. In order to achieve a high $K_u > 1.0 \times 10^7$ erg/cm^3 and a low $M_s < 120$ emu/cm^3, effect of repetition number (n), dependence of Mn content (x) and post annealing in $[Mn_x/Ge]_n$ multilayered films were investigated.

2. Experimental procedure

All of the $[Mn_x/Ge]_n$ multilayered films were fabricated on MgO (100) single crystal substrates by alternate sputtering method using an ultra-high vacuum magnetron sputtering system. The x was estimated from thickness ratio between Mn layers and Ge layers by using the density of manganese (α-Mn) 7.88×10^{28} atoms/m^3 and germanium 4.42×10^{28} atoms/m^3, respectively. The base pressure was below 8.0×10^{-6} Pa, and the Ar gas pressure was kept at 0.53 Pa during the deposition. The film structure was MgO (100) sub. / Cr buffer layer (5 nm) / $[Mn_x/Ge]_n$ multilayer (100 nm) / Cr protection layer (10 nm). After cleaning MgO (100) single crystal substrates by thermal processing in the sputtering chamber, the Cr buffer layer was deposited at room temperature on MgO (100) single crystal substrates. Subsequently, to obtain an atomically flat surface, the Cr buffer layer was annealed at 700°C. The $[Mn_x/Ge]_n$ multilayer was fabricated by alternate sputtering method using a Mn (3N) and a Ge (5N) target with total film thickness of 100 nm. The substrate temperature (T_s) was kept at 450°C during the deposition of $[Mn_x/Ge]_n$ multilayer. Finally, the Cr protection layer was deposited at room temperature. The analysis of crystal structure for $[Mn_x/Ge]_n$ films were performed by the X-ray diffraction (XRD). The magnetic properties of $[Mn_x/Ge]_n$ films were characterized by the super-conductivity quantum interference device (SQUID) in the field up to ±70 kOe at room temperature.

3. Results and discussion

First, to investigate crystal growth of the $[Mn/Ge]_{15}$ multilayered films, three samples which have film structures of (a) MgO (100) sub. / Cr (5 nm) / $[Mn/Ge]_{15}$ (100 nm) / Cr (10 nm), (b) MgO (100) sub. / Cr (5 nm) / $[Ge/Mn]_{15}$ (100 nm) / Cr (10 nm), and (c) MgO (100) sub. / $[Mn/Ge]_{15}$ (100 nm) / Cr (10 nm) were prepared. Fig. 1 shows XRD patterns and film structures of the each multilayered films. In the sample (a) of the $[Mn/Ge]_{15}$ on the Cr buffered MgO (100) substrate, (002) super-lattice and (004) fundamental diffraction peaks from $D0_{22}$-Mn_3Ge were clearly observed. On the other hand, (004) fundamental and (220) diffraction peaks were observed, but (002) super-lattice diffraction peak was not observed in the samples (b) and (c). These results suggest that both Cr buffer and depositing Mn layer first are effective for the formation of ordered $D0_{22}$-Mn_3Ge phase. Thus, turn of deposition which Mn layer deposited firstly was adopted afterward.

Fig. 2 shows XRD patterns of the $[Mn_x/Ge]_{15}$ (T_s = 450°C) multilayered films at various x. In the all $[Mn_x/Ge]_{15}$ samples with varied x, $D0_{22}$-Mn_3Ge (002) super-lattice and (004) fundamental diffraction peaks were clearly observed. It is confirmed that in the condition of $x \sim 3.2$, intensity of $D0_{22}$-Mn_3Ge (002) and (004) diffraction peaks were maximum. In the case of Mn poor at $D0_{22}$-Mn_3Ge diagram phase, it is suggesting that $D0_{22}$-Mn_3Ge phase was formed because of the occupation of Ge atoms in Mn sites for $D0_{22}$-Mn_3Ge crystal structure. Therefore, intensity ratio of $D0_{22}$-Mn_3Ge (002) and (004) diffraction peaks was decreased. On the other hand, in the condition of Mn rich, $D0_{22}$-Mn_3Ge phase was formed by Mn atom invaded Ge site. In the sample of x = 3.1 ($[Mn_{3.1}/Ge]_{15}$), most well oriented $D0_{22}$-Mn_3Ge single phase structure was obtained. M-H curves of the $[Mn/Ge]_n$ multilayer films were shown in Fig. 3. With increasing x, M_s was decreased. On the other hand, high coercivity H_c = 23.6 kOe was obtained at x = 2.8, however, difference between the M_s and remanent magnetization M_r was very large. These curves indicate the mixture of relatively soft phase and hard phase. From the magnetization curves, the $[Mn_{3.1}/Ge]_{15}$ multilayered film exhibited highest M_s = 140 emu/cm^3 in this study.

Fig. 4 shows relations among x, c/a and M_s for the $[Mn_xGe]_{15}$ films. From x = 2.8 to x = 3.1, c/a indicated approximately 1.910. At x = 3.1, the c-axis and the a-axis is estimated to be 7.23 Å and 3.79 Å respectively, and, the M_s showed a value (140 emu/cm^3) that was maximum in this study. And the degree of order S was estimated approximately 0.7 using a following relation.

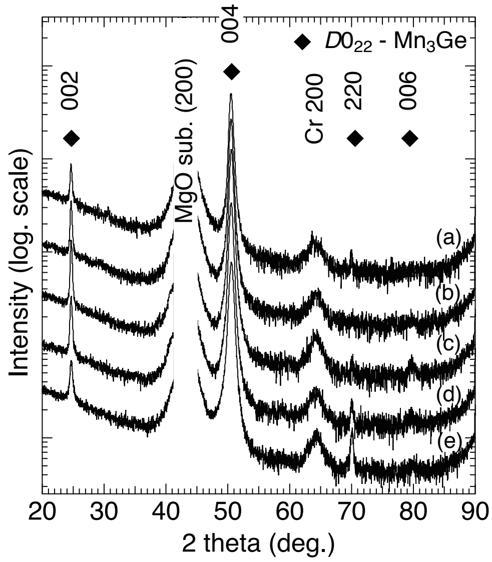

Fig. 2 XRD patterns for $[Mn_x/Ge]_{15}$ (T_s = 450ºC) multilayered films with varied Mn content (x). The Mn content (x) for $[Mn_x/Ge]_{15}$ multilayered films are 2.8 (a), 3.1 (b), 3.2 (c), 3.5 (d), 3.7 (e).

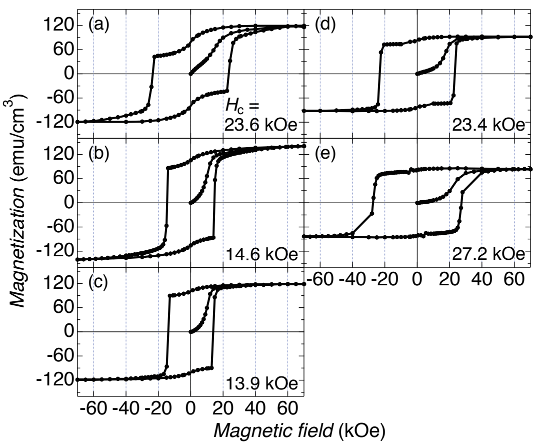

Fig. 3 M-H curves for $[Mn_x/Ge]_{15}$ (T_s = 450°C) multilayered films with varied Mn content (x). The Mn content (x) for $[Mn_x/Ge]_{15}$ multilayered films are 2.8 (a), 3.1 (b), 3.2 (c), 3.5 (d), 3.7 (e).

$$S = \frac{\sqrt{\frac{I_{exp.}(024)}{I_{exp.}(024)}}}{\sqrt{\frac{I_{calc.}(011)}{I_{calc.}(024)}}} \tag{1}$$

In the condition of Mn rich content, c/a showed 1.901 and M_s tended to decrease because the number of Mn atoms with anti-ferromagnetic coupling became large.

Fig. 5 shows XRD patterns of post annealing effect for the $[Mn_{3.5}/Ge]_{15}$ multilayered films. $D0_{22}$-Mn_3Ge (002), (006) super-lattice and (004) fundamental diffraction peaks were observed in both samples. In the post

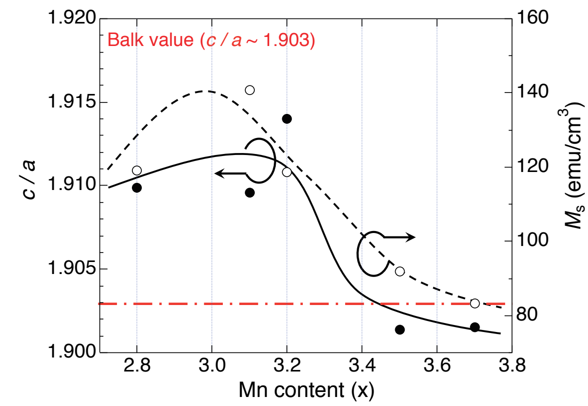

Fig. 4 c/a and M_s as function of Mn content (x) for $[Mn_x/Ge]_{15}$ multilayered films.

annealing condition of T_a = 500°C, it is thought that quality of the crystal become superior, because the diffraction intensity ratios between (002), (006) and (004) were increased.

Fig. 6 shows M-H curves after post annealing for the $[Mn_{3.5}/Ge]_{15}$ multilayered films. In the case of T_a = 500°C, M_s = 119 emu/cm^3 was observed. The square shape of the magnetization curves was improved by the post annealing. Steps of the M-H curve in Fig. 6 (a) nearby zero field were improved by post annealing at 500ºC (Fig. 6 (b)). The value of K_u of the $[Mn_{3.5}/Ge]_{15}$ multilayered films was estimated from perpendicular and in-plane magnetization curves of Fig. 6, which was estimated using the following equation.

$$K_u = \frac{H_k^{eff} M_s}{2} + 2\pi M_s^2 \tag{2}$$

Where H_k^{eff} is anisotropic field estimated by extrapolating the in-plane magnetization curve. In sample of (b), K_u was estimated to approximately 1×10^7 erg/cm^3.

Finally, the efficacy of the repetition number n was investigated for x = 3.5. Fig. 7 shows XRD patterns of the $[Mn_{3.5}/Ge]_n$ multilayered films with variation of n. The chemical content ratio of Mn was fixed as 3.5. On the conditions that n is more than 5, $D0_{22}$-Mn_3Ge (002) super-lattice and (004) fundamental diffraction peaks were observed clearly. Further, it is confirmed that highly ordered $D0_{22}$-Mn_3Ge phase was prepared in the $[Mn_{3.5}/Ge]_n$ multilayered films at n = 15-30. In this experiment, n was varied within constant total thickness of the film. In other words, deposition thickness at once became thinner with increasing n. As a sputtered film thickness becomes thinner at once, it is thought that $D0_{22}$-Mn_3Ge become easy to crystallize because internal mixing between Mn and Ge becomes easy. As the results, with increasing n, $D0_{22}$-Mn_3Ge (002) and (004) direction peaks intensities were increased. M-H curves of $[Mn_{3.5}/Ge]_n$ multilayered films were shown in Fig. 8. From magnetic properties, with increasing n, M_s was increased, however H_c was decreased. And M_s = 112

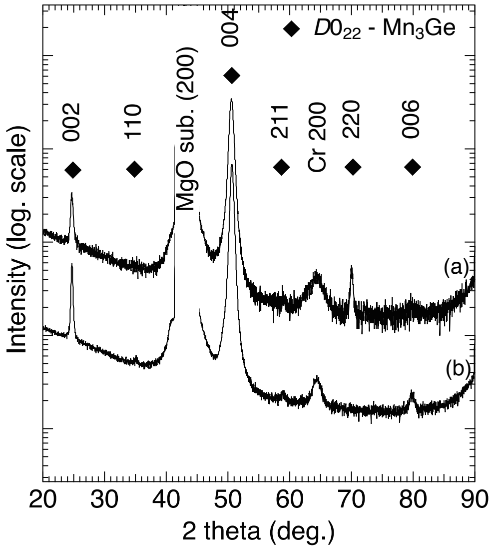

Fig. 5 XRD patterns for [$Mn_{3.5}$/Ge]$_{15}$ multilayered films.
(a) T_s = 450°C.
(b) T_s = 450°C, T_a = 500°C.

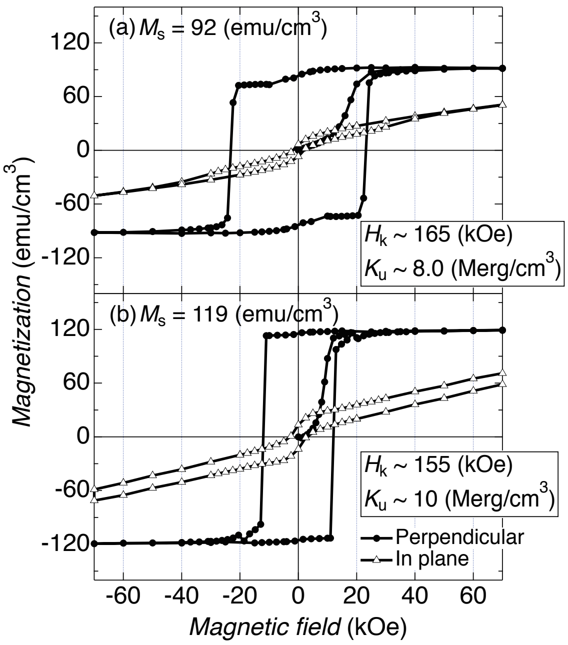

Fig. 6 *M-H* curves for [$Mn_{3.5}$/Ge]$_{15}$ multilayered films.
(a) T_s = 450°C.
(b) T_s = 450°C, T_a = 500°C.

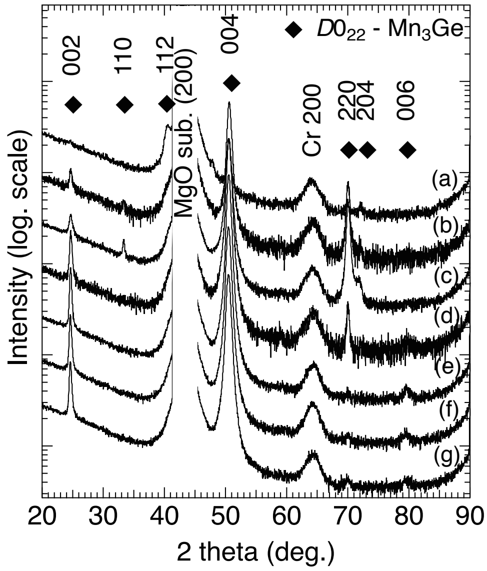

Fig. 7 XRD patterns for [$Mn_{3.3}$/Ge]$_n$ (T_s = 450°C) multilayered films with varied repetition number (n). The repetition number (n) for [$Mn_{3.5}$/Ge]$_n$ multilayer films are 1 (a), 5 (b), 10 (c), 15 (d), 20 (e), 25 (f), 30 (g).

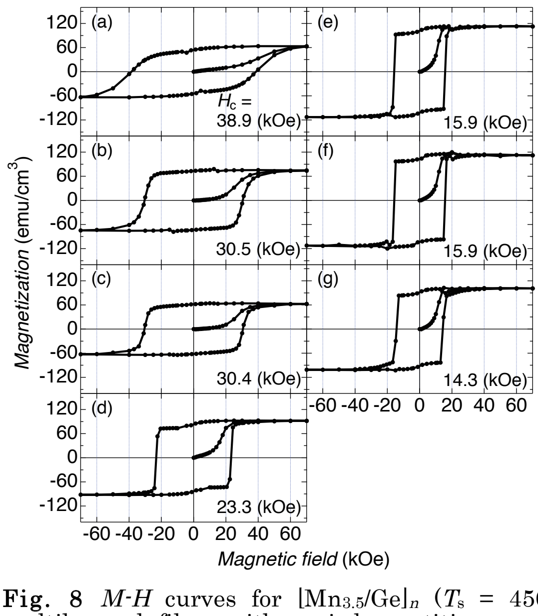

Fig. 8 *M-H* curves for [$Mn_{3.5}$/Ge]$_n$ (T_s = 450°C) multilayered films with varied repetition number (n). The repetition number (n) for [$Mn_{3.5}$/Ge]$_n$ multilayered films are 1 (a), 5 (b), 10 (c), 15 (d), 20 (e), 25 (f), 30 (g).

emu/cm^3 was observed on conditions that n is 20 and 25. It is confirmed that almost same thin film can be obtained without annealing by the increase of repetition number n. On the other hand, in the case of n is 1; Ge layer was deposited ~ 34 nm after Mn layer was deposited ~ 66 nm on the Cr buffer layer, a high H_c = 38.4 kOe was observed. In the XRD patterns of Fig. 7, $D0_{22}$-Mn_3Ge (002) super-lattice diffraction peak intensity was extremely low, however, (004) and (220) diffraction peaks were clearly observed at n = 1. It is considered that disordered $D0_{22}$-Mn_3Ge structure exist mainly at n = 1. Therefore, M_s showed a low value (63 emu/cm^3). At n = 1, each Mn and Ge sputtered film thickness were too thick to be crystallized for ordered $D0_{22}$-Mn_3Ge.

Fig. 9 shows relations among n, c/a and M_s for the

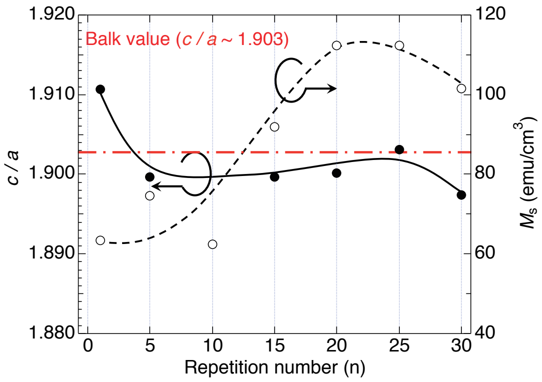

Fig. 9 *c/a* and M_s as function of repetition number (*n*) for $[Mn_{3.5}/Ge]_n$ multilayered films.

$[Mn_{3.5}/Ge]_n$ multilayered films. From $n = 5$ to $n = 25$, *c/a* indicated approximately 1.9. From the XRD profiles (n = 5- 25), it is thought that *c/a* showed same value of bulk because a (002) super-lattice diffraction peak and a (004) fundamental peak appeared and ordered $D0_{22}$-Mn_3Ge phase exist mainly. On the other hand, with increase *n*, M_s tended to increase. At n = 25, *c*-axis and *a*-axis indicated 7.22 Å and 3.80 Å respectively and because a *c/a* value showed a value (1.903) at the same level as the bulk value, the M_s showed the value (112 emu/cm^3) that was near to the bulk value. At n = 30, the *c*-axis indicated 7.23 Å and the *a*-axis indicated 3.81 Å. The M_s was 101 emu/cm^3 that was slightly lower than the M_s of n = 25 (112 emu/cm^3). Because the *M-H* curves in Fig. 6 (b) and Fig. 8 (e), (h) are almost same, and the XRD patterns, the *c/a* is also almost same to after post annealing at n = 15, 20, it is confirmed that increase of *n* by alternate sputtering method has a same effect of post annealing at 500ºC.

4. Summary

A Cr buffer layer played an important role in epitaxial growth on MgO (100) crystal substrates from fabrication of a $[Mn/Ge]_{15}$ multilayer. Highly oriented $D0_{22}$-Mn_3Ge phase was grown on a Cr buffered MgO (100) single substrate by deposition of a Mn layer onto the Cr buffer layer before deposition of a Ge layer. The squareness of magnetization curves for $D0_{22}$-Mn_3Ge was improved by post annealing process (T_a = 500ºC). $D0_{22}$-Mn_3Ge that having a high K_u ~ ca. 1.0×10^7 erg/cm3, M_s = 119 emu/cm^3 and good squareness for $[Mn_{3.5}Ge]_{15}$ (T_s = 450ºC, T_a = 500ºC) multilayer film was obtained by using alternate sputtering method, with post annealing. it is confirmed that increase of *n* by alternate sputtering method has a same effect of post annealing at 500ºC.

Acknowledgments This study was partly supported by Collaborative Research Based on Industrial Demand program from Japan Science and Technology Agency and a Grant-in Aid for Scientific Research (A).

References

1) K L Wang, J G Alzate and P Khalili Amiri: *J. Phys. D: Appl. Phys.* **46** (2013) 074003 (10pp).
2) H. Yoda, T. Kishi, T. Nagase, M. Yoshikawa, K. Nishiyama, E. Kitagawa, T. Daibou, M. Amano, N. Shimomura, S. Takahashi, T. Kai, M. Nakayama, H. Aikawa, S. Ikegawa, M. Nagamine, J. Ozeki, S. Mizukami, M. Oogane, Y. Ando, S. Yuasa, K. Yakushiji, H. Kubota, Y. Suzuki, Y. Nakatani, T. Miyazaki, and K. Ando: *Curr. Appl. Phys.*, **10** (2010) e87-e89.
3) H. Sato, M. Yamanouchi, S. Ikeda, S. Fukami, F. Matsukura and H. Ohno: *J. Magn. Soc. Jpn.*, Vol. **38**, No.2-2, 2014.
4) Y. Huai: *AAPPS Bulletin* December 2008, Vol. **18**, No. 6.
5) W. H. Bulter, X.-G. Zhang, T. C. Schulthess, and J. M. MacLaren: *Phys. Rev. B* **63**, 054416 (2001).
6) S. Ikeda, H. Yamamoto, K. Mizunuma, H. D. Gan, M. Endo, S. Kanai, J. Hayakawa, F. Matsukura, and H. Ohno : *Nat. Mater.*, **9**, 721-724 (2010).
7) Z. Kugler, J-P. Grote, V. Drewello, O. Schebaum, G. Reiss, and A. Thomas: *J. Appl. Phys.*, **111**, 07C703 (2012).
8) K. Yakushiji, T. Sayuya, H. Kubota, A. Fukushima, T. Nagahama, S. Yuasa, and K. Ando: *Appl. Phys. Lett.*, **97**, 232508 (2010).
9) D. Watanabe, S. Mizukami, F. Wu, M. Oogane, H. Naganuma, Y. Ando, T. Miyazaki: *J. Phys. Conf. Series* **200**, 072104-1-4 (2010).
10) S. Mizukami, X. Zhang, T. Kubota, H. Naganuma, M. Oogane, Y. Ando, and T. Miyazaki: *Appl. Phys. Express*, **4** (2011) 013005.
11) N. Inami, G. Kim, T. Hiratuka, H. Naganuma, M. Oogane, Y. Ando: *J. Phys. Conf. Series* **200**, (2010) 052008.
12) J. M. D. Coey: *J. Phys.: Condens. Matter*, **26** (2014) 064211 (6pp)
13) K. Wang, E. Lu, J. W. Knepper, F. Yang, and A. R. Smith: *Appl. Phy. Lett.*, **98**, 162507 (2011).
14) F. Wu, S. Mizukami, D. Watanabe, H. Naganuma, M. Oogane, Y. Ando, and T. Miyazaki: *Appl. Phys. Lett.*, **94**, 122503 (2009).
15) S. Mizukami, T.Kubota, F. Wu, X. Zhang, and T. Miyazaki, H. Naganuma, M. Oogane, A. Sakuma, and Y. Ando: *Phys. Rev.* B **85**, 014416 (2012).
16) H. Kurt, K. Rode, M. Venkatesan, P. Stamenov, and J. M. D. Coey: *Phys. Rev.* B **83**, 020405(R) (2011).
17) A. Sakuma: *J. Phys. Soc. Jpn.*, Vol. **63**, No. 4, April, pp. 1422-1428 (1994).
18) Y. Kota and A. Sakuma: *J. Phys. Soc. Jpn.*, **81** (2012) 084705.
19) M. Hosoda, M. Oogane, M. Kubota, T. Kubota, H. Saruyama, S. Iihama, H. Naganuma, and Y. Ando: *J. Appl. Phys.*, **111**, 07A324 (2012).
20) H. Saruyama, M. Oogane, Y. Kurimoto, H. Naganuma, and Y. Ando: *Jpn. J. Appl. Phys.*, **52**

(2013) 063003.
21) S. Wurmehl, H. C. Kandpal, G. H. Fecher, and C. Felser: *J. Phys.: condens. Matter* **18** (2006) 6171.
22) A. Sugihara, S. Mizukami, Y. Yamada. K. Koike, and T. Miyazaki: *Appl. Phys. Lett.*, **104**, 132404 (2014).
23) A. Sugihara, K. Z. Suzuki, T. Miyazaki, and S. Mizukami: *J. Appl. Phys.*, **117**, 17B511 (2015).
24) A. Sugihara, K. Suzuki, S. Mizukami, and T. Miyazaki: *J. Phys. D: Appl. Phys.*, **48** (2015) 164009 (5pp).
25) Y. Miura, and M. Shirai: *IEEE Trans. Magn.*, Vol. **50**, 1400504 (2014).

Received May 19, 2016; Revised Feb. 15, 2017; Accepted Mar. 27, 2018

Notice for Photocopying

If you wish to photocopy any work of this publication, you have to get permission from the following organization to which licensing of copyright clearance is delegated by the copyright owner.

〈All users except those in USA〉
Japan Academic Association for Copyright Clearance, Inc. (JAACC)
6–41 Akasaka 9-chome, Minato-ku, Tokyo 107–0052 Japan
Phone 81–3–3475–5618 FAX 81–3–3475–5619 E-mail: info@jaacc.jp

〈Users in USA〉
Copyright Clearance Center, Inc.
222 Rosewood Drive, Danvers, MA01923 USA
Phone 1–978–750–8400 FAX 1–978–646–8600

複写をされる方へ

本会は下記協会に複写に関する権利委託をしていますので，本誌に掲載された著作物を複写したい方は，同協会より許諾を受けて複写して下さい．但し（社）日本複写権センター（同協会より権利を再委託）と包括複写許諾契約を締結されている企業の社員による社内利用目的の複写はその必要はありません．（社外頒布用の複写は許諾が必要です．）

権利委託先：一般社団法人学術著作権協会
〒107–0052 東京都港区赤坂9–6–41 乃木坂ビル
電話（03）3475–5618 FAX（03）3475–5619 E-mail: info@jaacc.jp

なお，著作者の転載・翻訳のような，複写以外の許諾は，学術著作権協会では扱っていませんので，直接本会へご連絡ください．

Journal of the Magnetics Society of Japan

Vol. 42 No. 4 (通巻第 298 号) 2018 年 7 月 1 日発行

Vol. 42 No. 4 Published Jul. 1, 2018
by the Magnetics Society of Japan
Tokyo YWCA building Rm207, 1–8–11 Kanda surugadai, Chiyoda-ku, Tokyo 101–0062
Tel. +81–3–5281–0106 Fax. +81–3–5281–0107

Printed by JP Corporation Co., Ltd.
2–3–36, Minamikase, Saiwai-ku, Kanagawa 212–0055
Advertising agency: Kagaku Gijutsu-sha

発行：(公社)日本磁気学会 101–0062 東京都千代田区神田駿河台 1–8–11 東京YWCA会館 207 号室
製作：ジェイピーコーポレーション 212–0055 神奈川県川崎市幸区南加瀬 2–3–36 Tel.（044）571–5815
広告取扱い：科学技術社 111–0052 東京都台東区柳橋 2–10–8 武田ビル 4F Tel.（03）5809–1132